Molecular and Crystalline Microstructure of Ferroelectric Poly(vinylidene fluoride-*co*-trifluoroethylene) Ultrathin Films on Bare and Self-Assembled Monolayer-Modified Au Substrates

Youn Jung Park, Seok Ju Kang, and Cheolmin Park*

Department of Materials Science and Engineering, Yonsei University, Seoul 120-749, Korea

Bernard Lotz and Annette Thierry

Institut Charles Sadron (CNRS-ULP), 6, Rue Boussingault, 67083 Strasbourg, France

Kap Jin Kim

College of Environment and Applied Chemistry, Department of Advanced Polymer and Fiber Materials, Kyung Hee University, Yongin-si, Gyeonggi-do 449-701, Korea

June Huh

Department of Materials Science and Engineering, Seoul National University, Seoul 157-742, Korea

Received August 17, 2007; Revised Manuscript Received October 8, 2007

ABSTRACT: We investigate the molecular and microdomain structure of ferroelectric poly(vinylidene fluoride-*co*-trifluoroethylene) P(VDF−TrFE) copolymer thin films spin-coated on bare and self-assembled monolayers (SAMs)-modified Au substrates. The two types of films display similar crystal morphologies with edge-on needlelike shaped crystalline microdomains. They have, however, a different structure depending on the substrate. When the P(VDF−TrFE) films are deposited on a bare, unmodified Au surface, the P(VDF-TrFE) films preferentially have a (110) contact plane with the substrate but a (100) contact plane when deposited on the Au surface modified by SAMs. The polar *b*-axis, along which the ferroelectric polarization is oriented, is therefore tilted to the film (and substrate) surface normal at 30 and 90°, respectively. In particular, the orientation of the polar *b*-axis tilted at some 90° to the normal of the polymer films on a CH_3 terminated SAM modified Au surface explains the smaller remanent polarization at low initial electrical bias.

Introduction

Poly(vinylidene fluoride) (PVDF) and its copolymers with trifluoroethylene (TrFE) are polymeric materials with ferroelectric properties that are of particular interest for, e.g., nonvolatile memory device applications.[1−10] Ferroelectric polymer storage devices include a ferroelectric polymer thin film sandwiched between arrays of metal electrodes that makes possible electrical charge signaling across the structure. The polarization behavior depends mainly on the crystallinity and crystal orientation of P(VDF−TrFE) below its Curie temperature. However, electrical switching of P(VDF−TrFE) copolymers requires a relatively large coercive field of approximately 50 MV/m. In order to reduce the applied voltage, the films must be as thin as possible. For very thin films, capacitor performance depends critically on the interface between the metal electrode and polymer. Indeed, the film structure depends to a large extent on the nucleation and growth mechanisms that are significantly influenced by the infinitely large film interface relative to its thickness. Many earlier works have demonstrated a significant reduction of the degree of crystallinity when the film thickness reaches ∼50 nm, thus setting a practical limit below which the capacitor shows very poor remanent polarization. In nearly all these works, only the *overall crystallinity* of the film has been correlated with the polarization of the capacitor, without considering the *orientation* of the polymer crystals, or more exactly *the orientation of the crystal lattice* in the thin films.[8−10] This unit-cell orientation issue is however a major ingredient in the capacitor performance, as illustrated by the work of Xia et al.[10] These authors showed indeed that an in-plane lamellar orientation observed in an ultrathin P(VDF−TrFE) film on an Al substrate (i.e., with the chain axis normal to the film thickness) is ineffective for polarization switching under an electric field.

The impact of the bottom electrode is one of the most important issues in the ferroelectric polarization of a thin film P(VDF−TrFE) capacitor. Xia et al. related both polarization and dielectric leakage current of the capacitor to the work function of the bottom electrode.[11] Apart from this single report, only limited information is available on a possible link between the ferroelectric properties and the crystalline microstructure and molecular orientation, as they are influenced by the electrode surface roughness and surface energy. Our previous work has demonstrated the importance of the topology of the bottom electrode by employing a topographically nanostructured etched Al surface that gives rise to the high-temperature polarization recovery of a P(VDF−TrFE) capacitor compared to one with a flat Al bottom electrode.[12] This limitation may stem from the fact that a modification of the surface energy by using a different electrode modifies at the same time the physical and electrical properties (different work function, grain structure and size, etc). It is difficult to devise and fabricate a set of bottom electrodes with systematically varied chemical properties without altering their physical and electrical properties as well.

* Corresponding author. Phone: +82-2-2123-2833. Fax: +82-2-312-5375. E-mail: cmpark@yonsei.ac.kr.

10.1021/ma0718705 CCC: $40.75
Published on Web 12/12/2007

Table 1. Characteristics of Alkanethiolates Self-Assembled Monolayers

	chemical structure	water contact angle (deg)
octanethiol (OT)	$CH_3(CH_2)_6CH_2SH$	89
dodecanethiol (DDT)	$CH_3(CH_2)_{10}CH_2SH$	93
hexadecanethiol (HDT)	$CH_3(CH_2)_{14}CH_2SH$	103
O_2 plasma treated hexadecanethiol (HDT)	$CH_3(CH_2)_{14}CH_2SH$	23
16-mercaptohexadecanoic acid (MHA)	$COOH(CH_2)_{14}CH_2SH$	47

Insertion of a *molecular interlayer*, which can also interact with both the ferroelectric polymer and metal electrode, is one possible way to control the interface and resulting ferroelectric properties. Self-assembled monolayers (SAMs), i.e., ordered surfaces of organic layers which can be easily formed on the metal or metal oxide surface, have been used to control the interface of organic devices such as organic/polymer light emitting diode[13,14] and solar cells.[15,16] As of yet, the enhanced performance of organic devices that include SAMs is not clearly understood. However, the modification of crystalline organic molecules on SAMs could be one explanation.[17] Furthermore, SAM interlayers a few nanometers thick make it possible to modify the surface chemical properties by varying the terminal groups exposed to the surface without altering the topography significantly. Although it is reported that the interfacial dipole imposed by the SAMs' interlayer modifies the work function of metal electrode in an organic light emitting diode,[18] the work function change by the SAMs in our capacitors rarely influences the ferroelectric switching potential.

In the present contribution, we investigate the molecular and microstructure of thin crystalline P(VDF−TrFE) films deposited on a polycrystalline Au substrate. Two different unit-cell orientations were obtained for thin films deposited either on the bare Au substrate or the Au one modified by using SAMs. It is further shown that these structural differences induce different electric responses of the films.

Experimental Section

Au Electrodes and Their Modification with SAMs. Au deposited substrate by the sputtering technique 150 nm thick was purchased from INOSTEK, Korea. The alkanethiolates used to produce the SAMs were all ordered from Aldrich. They are hexadecanethiol (HDT), dodecanethiol (DDT), octanethiol (OT) (all CH_3 terminated), and 16-mercaptohexadecanoic acid (MHA) with a COOH terminal group. The Au-sputtered substrates were coated with the monolayers by immersion in their ethanolic thiol solutions (2 mM) for 24 h at room temperature, rinsed with ethanol, and dried under a stream of nitrogen. The characteristics of the alkanethiolates SAMs are summarized in Table 1.

Thin Film Preparation. The P(VDF−TrFE) copolymer with 27.5 wt % TrFE used in this study was kindly supplied by MSI Sensor, PA. The melting (T_m) and Curie (T_c) temperatures of the P(VDF−TrFE) copolymer are 150 °C and 80 °C, respectively. Thin films were made by spin coating 0.3∼3% P(VDF−TrFE) solutions in methyl ethyl ketone. The films' thicknesses range from 30 to 250 nm, as measured by ellipsometry (Gaertner Scientific Co.). Annealing of the films (typically at 135 °C for 2 h) was performed in a Linkam 600 heating stage.

Ferroelectric Polarization Measurement. Aluminum electrodes were evaporated on the polymer films' top surfaces using a mask with 200 μm diameter holes under a $\sim 10^{-6}$ mB pressure at a ∼0.1 nm/s deposition rate. Ferroelectric properties were determined using a virtual ground circuit (Radiant Technologies Precision LC unit).

Structure Characterization. The structure of the films was characterized by field emission scanning electron microscope (FESEM, Sirion) and by two-dimensional (2D) grazing-incidence wide-angle X-ray scattering (GIWAXS). The latter experiments were performed on the 4C2 beam line at the Pohang Accelerator Laboratory in Korea (incidence angle: 0.09°∼0.15°). The samples were mounted on an *x* and *y* axes goniometer. Monochromatized X-rays ($\lambda = 0.1608$ nm) under vacuum and the full range of available incidence angles were used. The scattered beam intensity was recorded with an SCX: 4300−165/2 CCD detector (Princeton Instruments). 2D GIWAXS patterns were obtained in the range $0 < q_z < 2.33$ Å^{-1}, $0 < q_{xy} < 2.33$ Å^{-1}($q = 4\pi \sin\theta/\lambda$, with *z* perpendicular and *xy* parallel to the substrate).

From the azimuthal scans, we calculated the orientation factors to interpret the diffraction results more quantitatively. The degree of alignment of the characteristic reflections depending on the substrates was quantified using the second-order orientation factor, *f*.[19] The diffraction intensity was integrated as a function of the azimuthal angle, ϕ in a ring about the principal peak wavevector q^*, with a width given by the full width at half-maximum of the primary peak, resulting in the scattered intensity as a function of angle, $I(q^*,\phi)$. The normalized orientation distribution function of a reflection is

$$P(\phi) = \frac{I(q^*,\phi)q^{*2}}{\int_{\theta_1}^{\theta_2} I(q^*,\phi)q^{*2} \sin\phi \, d\phi}$$

Herman's orientation factors (*f*) are given by

$$f = \frac{3\langle\cos^2\phi\rangle - 1}{2}$$

where $\langle\cos^2\phi\rangle$ is

$$\langle\cos^2\phi\rangle = \int_{\theta_1}^{\theta_2} \cos^2\phi P(\phi) \sin\phi \, d\phi$$

For a perfect orientation, $P(\phi)$ would be a delta function at 0° and $f = 1$. If the alignment is isotropic, $P(\phi)$ is independent of ϕ and $f = 0$.

Unpolarized Fourier transform infrared-grazing incident reflection absorption spectroscopy (FTIR-GIRAS) data were obtained using a Bruker-IFS66V spectrometer. Acquisition was made for 300 scans with an incident angle of approximately 80° from the normal to the substrate surface at a resolution of 2 cm^{-1}. Grazing incidence is mandatory for thin films: for the given incidence angle, the illuminated surface area is 3−30 times larger than for conventional transmission IR at normal incidence.

Results and Discussion

1. Morphology and Structure of the Thin Films. The structure of the thin films deposited on the Au and SAM-modified Au substrates have been examined by FESEM, GIWAXS, and GIRAS. FESEM investigations do not indicate any major *morphological* difference between films deposited on bare and on SAM-modified Au, but do underline systematic variations with film thickness, which become more pronounced for the thinner films.

The surface of a film approximately 250 nm thick is shown in Figure 1a. It displays typical edge-on, closely packed crystalline microdomains with needlelike shape. The individual needles are oriented randomly and away from the film surface. Each individual needlelike micro-domain, approximately 250 nm long and 50 nm wide, is composed of multiple stacks of crystalline lamellae ≈10 nm thick, as shown in the inset of Figure 1a. The *c*-axis of the P(VDF−TrFE) crystals, which is the molecular chain axis, is parallel to the Au substrate along the longitudinal direction of the needlelike microdomain as illustrated in the scheme shown in the inset of Figure 1b (an orientation also confirmed by GIWAXS, as seen soon), confirmed by the birefringence experiment. In order to identify the

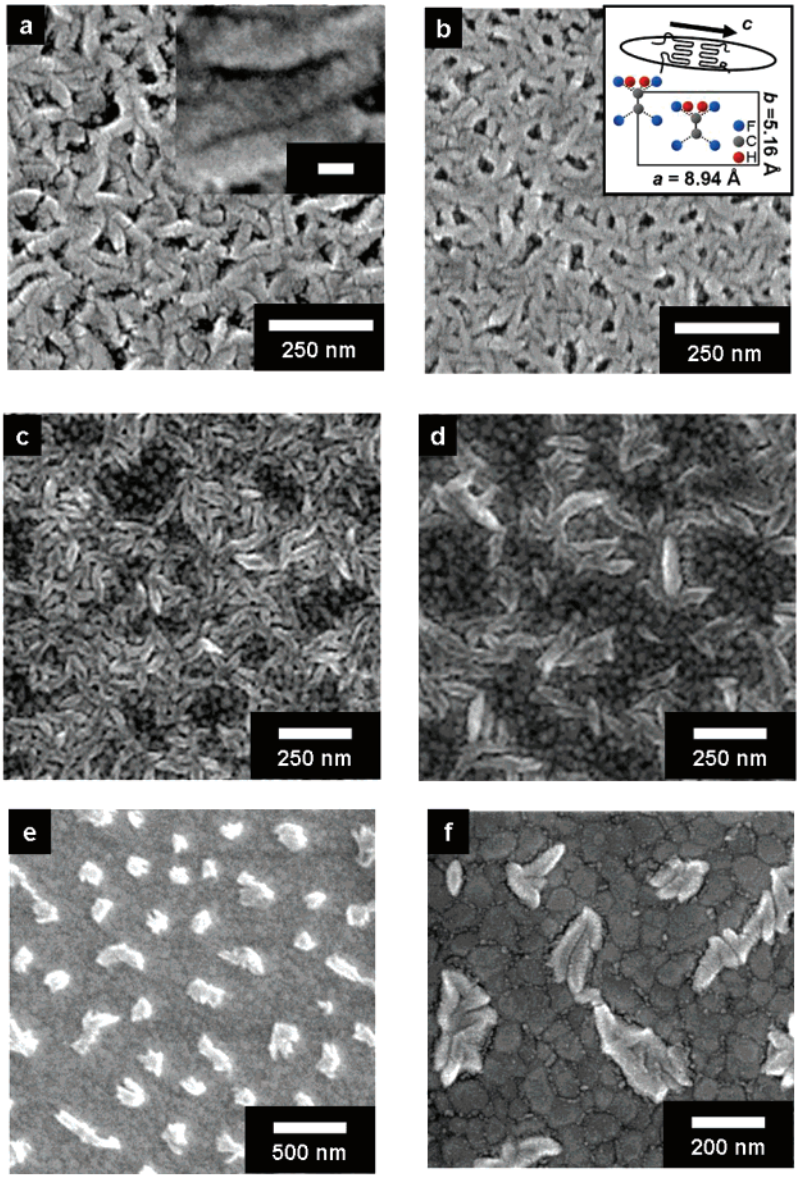

Figure 1. FESEM images of P(VDF−TrFE) films on the Au surface with various film thickness. (a) 250 nm, (b) 110 nm, (c) 30 nm, and (d) less than 30 nm. The inset image of part a shows the multistacking of lamellae in a needlelike crystalline microdomain. A scheme of the microdomain and the unit-cell of a P(VDF−TrFE), projected along the *c*-axis ($c = 2.55$ Å), are shown together in the insets of part b. The scale bar in the inset of part a is 40 nm. The aggregated needlelike morphology of the thin film was observed when 20 nm of the ultrathin film was formed on a (e) DDT- and (f) HDT-modified-Au surface. The distribution of needlelike microdomains differs in ultrathin polymer films on a Au surface with and without modification by SAMs.

birefringence sign of needlelike lamellar crystal, it is necessary to obtain as large of a needlelike lamellar crystal that can be observed on the polarizing microscope under cross polarization. We monitored the polarizing microscopic image during melt-crystallization of the 50 μm thick cast-sample on a glass slide at 143 °C. The needlelike lamellar crystal whose long axis is oriented along the two diagonal axis directions making angles of 45° and 135° with the polarization direction of a polarizer was seen brightest with a gray color equivalent to a retardation of about 170 nm. Along the diagonal axis having an angle of 45° with a polarizer direction, we inserted a first order red plate whose retardation is 530 nm with a slow direction perpendicular to the insertion direction. As a result, the needlelike lamellar crystals oriented making an angle of 45° with a polarizer were seen in blue color equivalent to a retardation of about 700 nm, whereas the needlelike lamellar crystals oriented making an angle of 135° with a polarizer were seen in yellow color equivalent to a retardation of about 360 nm. Therefore, the long axis of the needlelike crystal can be parallel to the slow direction of the first order red plate; thus, the needlelike crystal has a positive birefringence sign and the long axis of the needlelike crystal is also parallel to the molecular chain axis as seen in the inset of Figure 1b. The needlelike crystal is composed of multiple stacks of crystalline lamellae along the long axis direction.

As shown in Figure 1b, the film surface morphology remains essentially similar when the film thickness is only 110 nm but is drastically altered for ultrathin films of P(VDF−TrFE) (when the film thickness is less than 50 nm), as shown in Figure 1c. In the latter case, although the aggregates of needlelike P(VDF−TrFE) microdomains are still visible in some areas, these microdomains no longer cover the whole surface of the underlying substrate. Indeed, Au grains $\approx$ 30 nm in diameter can be seen distinctly around the aggregates of the polymer crystals. When the film thickness is reduced even further (to an average of less than 30 nm), the regions in which polymer

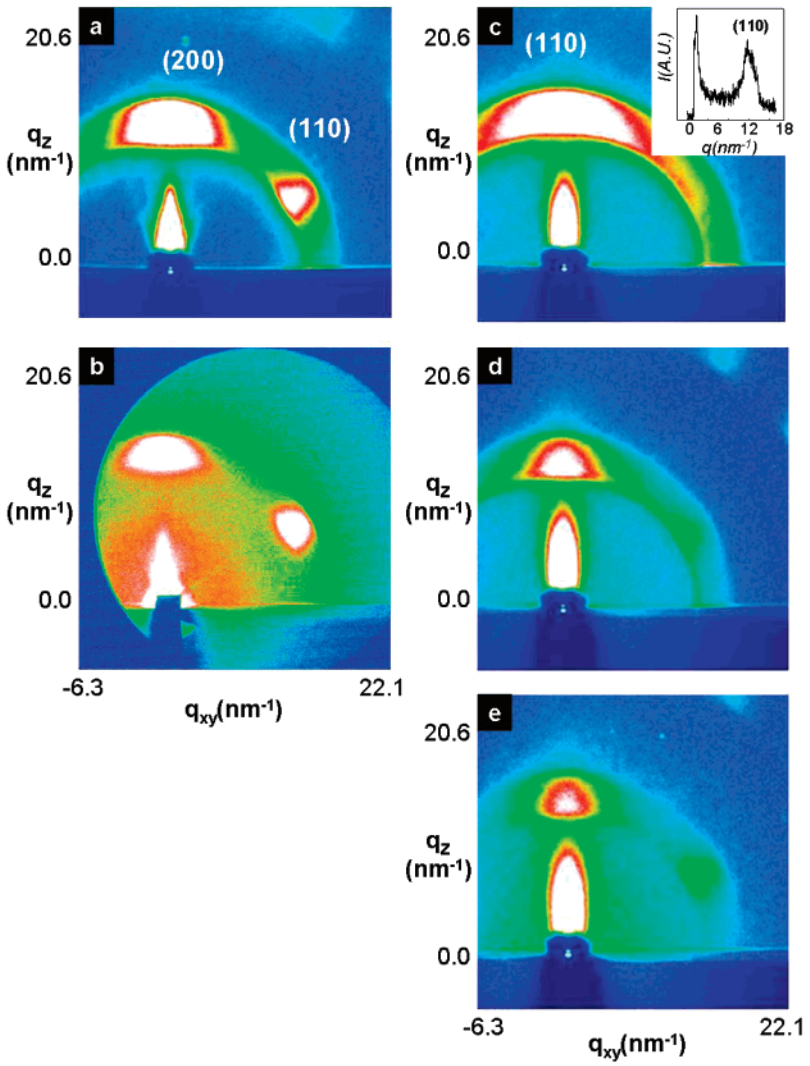

Figure 2. 2D GIWAXS patterns for P(VDF−TrFE) thin films on a HDT-modified-Au surface (a, b) on a bare Au surface (c−e) with different thickness. Patterns from (a) 250 nm and (b) 30 nm films display two strong reflections near 12 nm^{-1} on the meridian and 60° away from the meridian. (c) 250 nm, (d) 110 nm, (e) 30 nm, and the inset of part c display the intensity profile along the meridian direction. The strong reflection on the meridian exists for all thicknesses. The diffraction peak at 60° away from the meridian is absent in part c but has very weak intensity in the thinner films (parts d and e).

crystals are packed together cover at most half of the substrate surface, as shown in Figure 1d. Contrary to the morphology observed in the P(VDF−TrFE) thin film prepared by the Langmuir−Blodgett method in which nanosize dots and wells are formed, depending on the layer thickness,[20,21] the size and shape of the crystals that build up the thin films remain nearly similar regardless of the film thickness. Their *distribution* differs however for the thinner films deposited on Au and HDT-modified Au substrates. Indeed, for reasons that are not yet known, several microdomains are clustered in small packets on Au but are individually dispersed on the SAM-modified ones in Figure 1e,f.

In spite of their similar morphology, the films produced on "bare" Au and on HDT-modified Au have significantly different *structures*, as revealed by GIWAXS. The corresponding patterns are illustrated in Figure 2a,b,c−e for SAM-modified and bare Au substrates, respectively. In both cases, films with three different thicknesses are investigated, namely, 250, 110, and 30 nm. *All* films investigated display a strong or very strong reflection at 12 nm^{-1} (i.e., ≈4.6 Å) on the "meridian" of the diffraction pattern. However, the films deposited on SAM-modified Au and on the "bare"-Au substrate differ in either the presence or the virtual absence of reflections with nearly the same 12 nm^{-1} spacing some 60° away from that meridian.

First of all, analysis of this difference requires a short summary of the PVDF β phase diffraction characteristics.[22,23] We examined the structure factors based on the azimuthal intensity profiles of the GIWAXS results. The crystal structure of the P(VDF−TrFE) copolymer is generally considered an orthorhombic lattice (space group $Cm2m$). The systematic absence of the (hkl) reflections with $h + k = 2n$, characteristic of a centered lattice, is observed. Each observed peak consists of two or more overlapping Bragg reflections due to the pseudo-hexagonal nature of the structure which in turn results in nearly equal (200) and (110) spacing. The intensities $I(hkl)$ include the geometric Lorentz Factor $L(\theta) = 1/\sin^2(\theta_{(hkl)}) \cos(\theta_{(hkl)})$, the diffraction angle ($\theta_{(hkl)}$), and the multiplicity $m(hkl)$ of the (hkl) reflection. The superposition of two first-order peaks, respectively, (110) and (200), gives the same angle of 19.8°. By the equation, it can be concluded that the more intense $q = 12$ nm^{-1} peak results from the multiplicity factor. The value of the multiplicity factor depends on the crystal system. Thus the multiplicity factor for the (110) plane of an orthorhombic cell is 4 and for the (200) plane it is 2.[24] Therefore, the (110) is

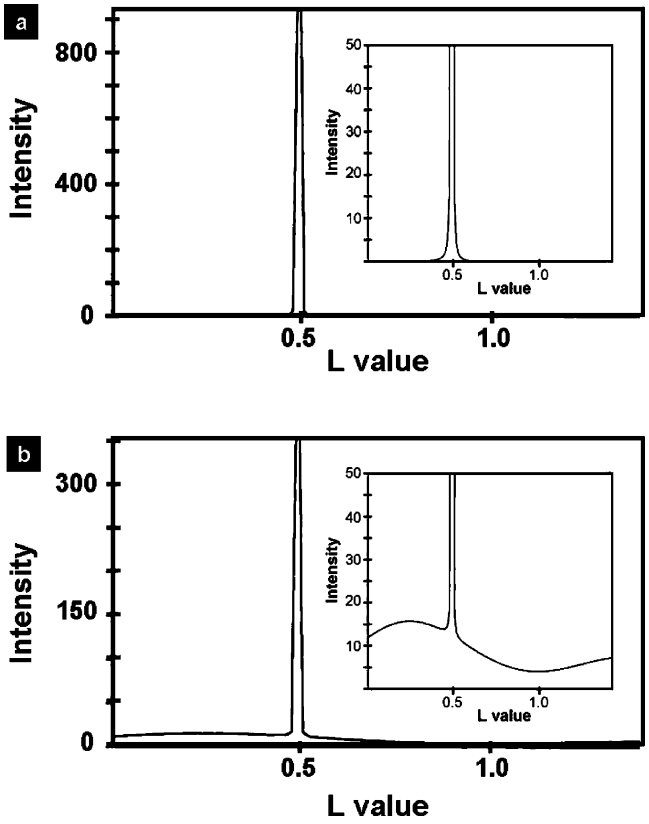

Figure 3. Modelization of the impact of the structural disorder introduced by twinning in the P(VDF−TrFE) films. The profiles are shown when (a) there is no disorder and (b) the orientations of the two *a*-axes in the twin are relative to the film normal. The insets have been set to have the maximum intensity at 50, in order to better visualize streaks.

stronger than the combined (200) reflections, which is consistent with our results shown in Figure 2a,c. The total intensity of the combined (110) and (200) in Figure 2c is higher than the (200) reflection in Figure 2a. In addition, the fact supports our model that in Figure 2a, the intensity of one of the 4-fold (110) reflections is comparable to that of one of the 2-fold (200) ones. As a consequence, although the patterns are distinctly different, it is difficult to unambiguously index the meridional and off-meridional reflections in Figures 2c∼e. The fact that the patterns are indeed different, however, suggests that the meridional reflections are different, i.e., (110) and (200) that the films deposited on the Au and on the SAM-modified Au differ by the nature of their contact planes. We further assume (anticipating the outcome of the analysis to be developed next) that the (110) face is preferentially in contact with the bare Au, whereas it is the (200) face for the SAM-modified one.

Why are the off-meridional reflections in the films deposited on bare Au so weak? Two possibilities may be considered, either that are linked with the structure of the deposited material or that indicate a difference in the film morphology.

Exploring possible differences in structure, one may first consider a structural disorder associated with multiple twinning in the film. If the contact plane with the substrate is indeed {110}, the two possible contact planes (110) and ($\bar{1}$10) may be involved. Their combination in any one crystallite results in a twinning, i.e., in a structural disorder that reduces the intensity of the off-meridional reflections (but not the meridional reflection, since it is parallel to the twin plane). The crystallographic disorder thus introduced would show up in the development of streaks, with concomitant reduction of the main reflection's intensity. The likelihood of such a crystallographic disorder has been checked by using the "Diffraction Faulted" module of the Cerius package.[25] The results are illustrated in Figure 3. It appears that the perturbation introduced by twinning reduces only marginally the main reflection's intensity and generates only a limited streaking. This limited impact stems from the fact that, although the orientations of the two *a* axes in the twin are symmetrically related relative to the film normal, the position of the chains in the twinned parts of the composite crystal is not significantly modified, as expected from the pseudo-hexagonal arrangement of the helices in the unit-cell. The modeling thus provides an unambiguous answer: a crystallographic disorder cannot account for the significantly reduced intensity of the off-meridional reflections in the films deposited on "bare" Au.

Since crystallographic features cannot explain the observed difference, one must consider the impact of morphological features, and more precisely of the tendency of lamellar crystals of PVDF to twist, as developed now. Here again, a short analysis of lamellar twisting in polymer crystal growth is in order.

Lamellar twisting is a frequent feature in polymer crystal growth, in particular from the melt.[26] Although the origin of lamellar twisting is still a matter of debate, it is likely that it is due to the existence of unbalanced surface stresses, associated with different fold structure/conformation, etc. Lamellar twisting is a standard feature in spherulites of PVDF in its α crystal modification (the γ phase spherulites are made of scrolled lamellae).[27−30] For pure PVDF, the β phase is produced only by mechanical deformation,[31] and no "spontaneous" morphology is known. To the best of our knowledge, the lamellar morphology of the bulk crystallized β phase of P(VDF−TrFE) copolymers has not been documented. Therefore, the three-dimensional shape of the lamellae in spherulites of the P(VDF−TrFE) copolymer of interest in this study has been examined, relying on well-established morphological features developed in earlier studies of other systems such as polyethylene, aliphatic polyesters, etc.[26]

The corresponding data are illustrated in Figure 4a,b. The optical micrograph of the film under polarized light in Figure 4a shows a concentric and periodic banded structure in an individual spherulite, for example, as indicated by an arrow which arose from the periodic birefringence modulation from the center of a spherulite by the cooperative twisting of the crystalline lamellae. A more telling illustration is provided by spherulite growth observed by AFM. Figure 4b shows an AFM image of the surface morphology of P(VDF−TrFE) spherulites grown in thin films. It displays curved edges of lamellae included in stacks, which is a classical indicator of lamellar twisting. Whereas these AFM and OM observations indicate that the P(VDF−TrFE) lamellae tend to twist, they do not, however, tell about which crystallographic axis the twist takes place. One can reasonably assume that it is the *a*-axis of the unit-cell, which would be the radial axis in a β phase spherulite. It should be noted that although the crystal rotation around the *a*-axis of the P(VDF−TrFE) crystals we proposed in our model was rationalized with the morphology of micrometer-thick films observed by both optical and AFM images shown in Figure 4, the 200 nm or less thick films do not exhibit clear evidence of the twisting *a*-axis mainly due to the short crystalline needlelike microdomains. As shown in Figure 4, the microstructral indication of lamellae twisting resulting from the crystal rotation occurs with the periodicity of approximately a few micrometers that is hardly visualized with the hundreds of nanometer long needlelike crystalline microdomains observed in FESEM in

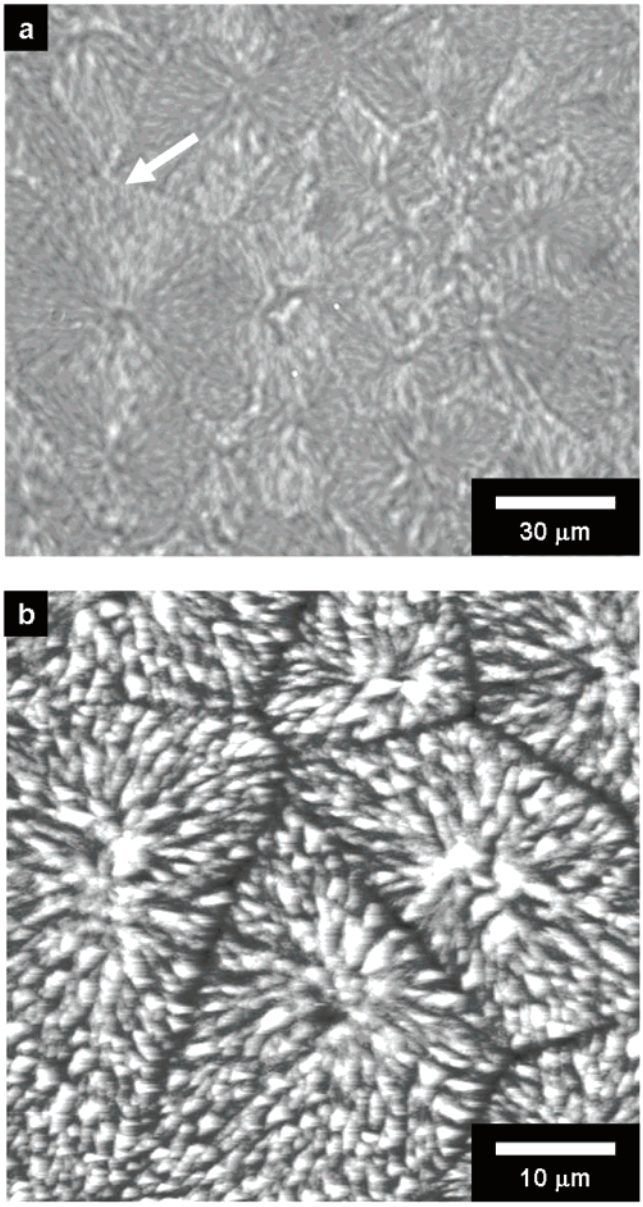

Figure 4. (a) An optical micrograph image under crossed polarizers illustrates the crystalline structure of P(VDF−TrFE) films crystallized at 148 °C for 24 h in 1 μm thick films with the small amount of additive, polymethyl methacrylate, to reduce the density of nuclei in the sample. A concentric and periodic morphology growing radially from the center is shown in the spherulites, as indicated by an arrow. These banded spherulitic images are one of the indicators of lamellar twisting. (b) Phase contrast-AFM image of the surface morphology of P(VDF−TrFE) spherulites. The curved edges of lamellae confirm lamellae twisting cooperatively in the spherulites.

Figure 1. The crystalline lamellae become longer with the film thickness. We do believe that the characteristic rotation around the *a*-axis is always present regardless of film thickness, but its microstructural evidence seems to be observed in a thick film with sufficiently long crystalline lamellae in Figure 4.

Having established that P(VDF−TrFE) lamellae tend to twist, we now examine the possible impact of this twisting on the diffraction pattern of thin films. For this purpose, it is convenient to consider first the films deposited on SAM-modified-Au substrates before tackling the more complex analysis of films deposited on bare Au. Furthermore, in order to ease the analysis, it is convenient to locate the reflections on a hemisphere where the positions of the reflections will thus be located on, e.g., the 30th parallel or the north pole (the latter corresponding to the meridional reflection) (Figure 5).

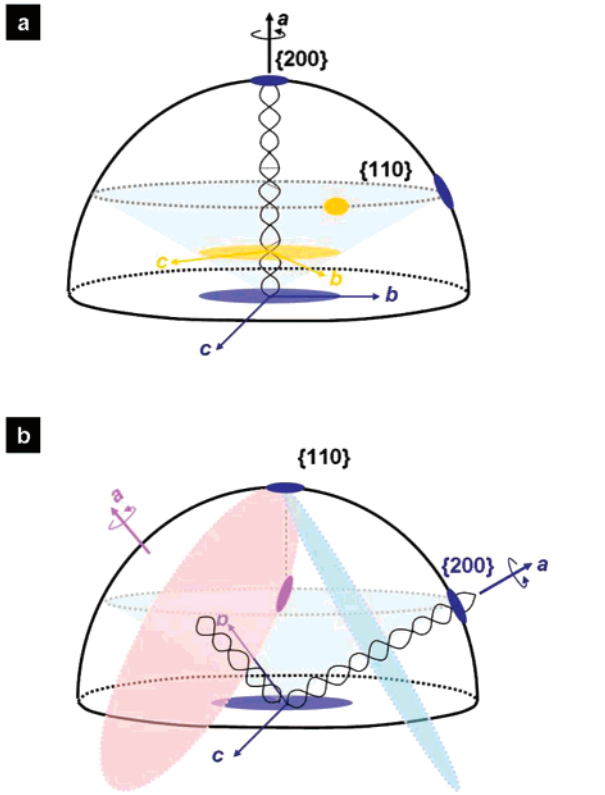

Figure 5. Schematic of the diffraction patterns in P(VDF−TrFE) with two different contact planes on the Au surface. (a) On CH_3-SAM-modified surfaces, the diffraction located on the meridian is indexed as (200). The lamellae twist around the *a*-axis spreads the {110} reflections over all azimuthal orientations, but they remain on the 30th parallel (a similar spread results from the lack of orientation of the crystallites in the film). (b) For films deposited on bare Au, the contact plane is (110) and the *a*-axis is tilted at 60° to the north pole. The strong {110} reflection is located at the north pole and the (200) and {110} reflections are spread over a wide part of the sphere.

In the thin films, the chains of P(VDF−TrFE) lie parallel to the substrate, but there is no preferred orientation of the chains within this plane: all azimuthal orientations are possible. In other words, the GIWAXS patterns correspond to some form of "fiber" patterns, in which the reflection corresponding to planes initially parallel to the substrate are on the north pole (meridional in fiber patterns) whereas the other reflections are located on layer lines. As is well-known from fiber diffraction work, the latter reflections are, for geometrical reasons, intrinsically weaker than the meridional reflections since only a fraction of the planes are in a diffracting position. In the analysis, we assume again that the contact plane differs for the two different substrates, (100) for SAM-modified Au and (110) for bare Au.

For films deposited on SAM-modified Au, the reflection located on the north pole is (200), and the (110) and ($\bar{1}$10) reflections are spread over all azimuthal orientations on the 30th parallel, in view of the fiber symmetry (lack of preferred orientation of the *c*-axis in the plane of the substrate). If the lamellae twist about the *a*-axis as they grow away from the substrate, the *c*-axis rotates about the *a*-axis that is normal to the film surface; this twist introduces merely a disorientation of the *c*-axis about the north pole direction, which was already present in the film, since there is no preferential orientation of the *c*-axis in the plane of the film to start with. In other words, the twisting of the lamellae introduces the same type of disorder that existed in the film, i.e., it has no impact on the GIWAXS

Table 2. Ferroelectric Properties and Characteristics in 2D GIWAXS Patterns from P(VDF−TrFE) Films Dependent on Thickness and SAMs

thickness/SAMs	FWHM[a]	*f* 110	remanent polarization[b] (P_r, μC/cm^2) (at 20 V)	coercive voltage (E_c, V) (at 20 V)	coercive field (E_c, MV/m)
250nm/bare Au		0.51	8.35	10.7	42.96
110nm/bare Au		0.68	11	7.27	66.09
70nm/bare Au		0.79	8.33	4.95	70.71
250nm/HDT	8.96	0.91	8.11	11.2	44.8
250nm/DDT	11.2	0.73	8.05	11.6	46.4
250nm/OT	14.56	0.56	8.08	12	48

[a] Full Width at Half Maximum (FWHM) value was calculated from the off-meridional peak. [b] The mean value from three different samples.

pattern. The pattern of the SAM-modified film is not sensitive to lamellar twisting and remains a "standard" fiber pattern, with the (200) reflection on the north pole and the combined (110) and ($\bar{1}$10) reflections spread on the 30th parallel as illustrated in the schematic of Figure 5a.

The situation is more complex for films deposited on bare Au, for which the (110) is the contact plane and the *a*-axis is titled at 60° to the north pole. Initially, the (110) reflection is located at the north pole, whereas the (200) and ($\bar{1}$10) reflections are spread on the 30th parallel north and south, respectively. Twisting about the *a*-axis in any one crystallite has a complex result. The *a*-axis remains oriented toward the 30th parallel (this may be a simplifying assumption, as developed later), but the (110) and ($\bar{1}$10) reflections rotate at 60° to this orientation (Figure 5b). For any one *a*-axis orientation, these reflections are therefore spread on a circle over a wide angular range that goes from the north pole to the 30th parallel south. Since, in addition, the *a*-axis adopts all azimuthal settings, the (110) and ($\bar{1}$10) reflections are spread on a significant fraction of the hemisphere, namely, between the north pole and the 30th parallel south. For obvious reasons of symmetry, the ($\bar{1}\bar{1}$0) and (1$\bar{1}$0) reflections are symmetrically related and are spread between the South pole and the 30th parallel north one. The feature of interest in this spread is that, although the angular range is quite large, all the circles described by these reflections pass through the north (or south) pole. In other words, the reflection observed on the meridian of the diffraction pattern arises in part from the contribution of each and every crystallite in the film, which explains its strength.

In this simplified version, the (200) reflection (which is anyhow weaker than the (110) reflection) would be spread over the 30th parallel. However, lamellar twisting is intrinsically a double twist, which introduces an additional angular spread. In addition, it is probable that during growth through the thickness of the film, the orientation of the *a*-axis progressively departs from the strict 60° tilt and tends toward the film normal, i.e., tends toward a kind of transcrystalline growth, which would reduce even further the intensity of reflections on the 30th parallel. This analysis is in line with the fact that, for the thinner films, the reflection on the 30th parallel is indeed relatively stronger (Figure 2e). We quantitatively characterized GIWAXS data to get orientation factors with respect to the film thickness. The improved orientation with the decrease of film thickness shown in Figure 2c−e was first quantified with the calculated orientation factors of the combined (110) and (200) reflections. *f* values for the films of 250, 110, and 30 nm in thickness were 0.51, 0.68, and 0.79, respectively. In addition, the orientation of the (110) reflection inclined to 60° with respect to the normal of the CH_3−SAMs-modified-Au surface was also estimated by the orientation factor (Table 2).

The combination of (a) a (110) contact plane (which results in the 60° tilt of the *a*-axis to the film normal) with (b) lamellar twisting thus provides a single and common structural and morphological frame that accounts for the unusual pattern of P(VDF−TrFE) films deposited on bare Au and for the difference with the films deposited on HDT-SAM-modified Au. For the former films, the striking, virtual disappearance of the reflections at 60° to the film normal does not mean that these reflections are absent but rather that they are spread over a very wide angular range. The above structural analysis is mainly based on diffraction evidence.

In addition to the HDT-modified substrate, we examined the molecular structures of 250 nm thick P(VDF−TrFE) films modified on Au substrates with OT and DDT. The characteristic reflection located at approximately 60° from the meridian also appeared in all films as shown in Figure 6a∼c. Furthermore, we found that the fwhm from the azimuthal intensity of this additional off-meridian reflection decreases with increased length of molecules of SAMs from OT and DDT to HDT as shown in Table 2. Again, the {110} reflection at approximately 60° from the meridian occurs when the *a*-axis is perpendicular to the substrate. The preferred orientation of P(VDF−TrFE) crystals on the substrate treated with CH_3-terminated SAMs implies that the crystal surface of the closely packed CH_3-terminated-SAM surface is more compatible with the (100) plane of the P(VDF−TrFE) crystals. Considering the fact that HDT forms the most stable monolayer with minimum surface defects among the SAMs we applied due to the strongest van der Waals interaction between alkyl backbones,[32] the highest orientation based on fwhm data (Table 2) in Figure 6c confirms the preferential (100) plane interaction with the CH_3-terminated-SAM surface. We also estimated the orientation factors to get the degree of orientation in {110} reflections in Figure 6. The *f* value of a film on an HDT modified surface was the largest among the films on other CH_3-SAMs-treated surfaces, as shown in Table 2. The calculated values are 0.91, 0.73, and 0.56 for HDT, DDT, and OT, respectively.

Confirmatory evidence in favor of the above structural analysis using FTIR-GIRAS data is shown in Figure 7 for ∼200 nm thick (annealed) films prepared on different substrates: (a) bare Au, (b) HDT/Au, (c) MHA/Au. As mentioned in our previous publication,[33] unpolarized GIRAS with the IR incident angle closer to the grazing incident angle (approximately 80∼88° from the surface normal) exhibits an enhanced p-polarized component (E_P) of the vibrational mode whose electric vector is perpendicular to the metal substrate surface and corresponds to a decrease in the s-polarized component (E_S) whose electric vector is parallel to the surface, as described before.[31] At the 80° incident angle used in this study, GIRAS predominantly detects the vibrational modes with the transition dipoles normal to the substrate surface and, hence, can be useful in clearly identifying the changes in the dipole and chain orientation. All the samples used in this study exhibited characteristic peaks; for example, the 1294 cm^{-1} band (A_1, $\vec{\mu} \parallel \vec{b}$) for the VDF trans sequence longer than TTTT, the 856 cm^{-1} band (A_1, $\vec{\mu} \parallel \vec{b}$) for the trans sequence longer than TTT, and the 1210 and 895 cm^{-1} bands (B_2, $\vec{\mu} \parallel \vec{a}$) associated with the crystalline phase showed relatively higher absorbance when

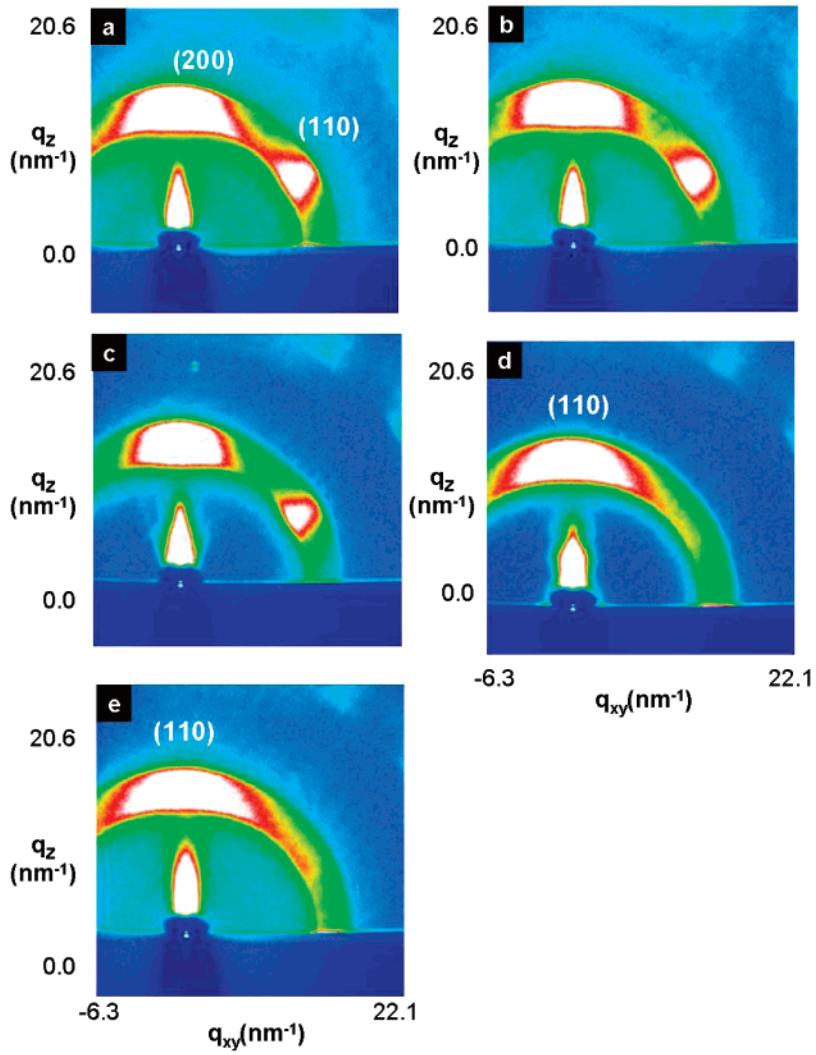

Figure 6. 2D GIWAXS patterns for 250 nm thick P(VDF−TrFE) thin films deposited on a Au surface modified with various SAMs: (a) OT, (b) DDT, (c) HDT, (d) MHA, (e) O_2 plasma treated HDT. The contact plane is (200) for films on a Au surface modified with hydrophobic SAMs. By contrast, the diffraction pattern of films formed on the hydrophilic surface indicates (110) contact planes.

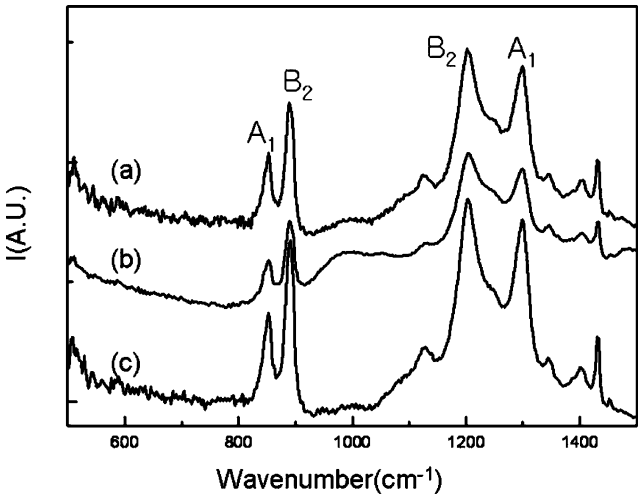

Figure 7. GIRAS spectra of P(VDF−TrFE) thin films spin coated on different Au substrates after annealing at 135 °C: (a) bare Au, (b) HDT/Au, (c) MHA/Au. The spectra are arbitrarily shifted for clarity.

compared to the 1402 cm^{-1} (B_1, $\vec{\mu} \parallel \vec{c}$) peak. This B_1 peak is assigned to ωCH_2 coupled with $\nu_{as}C-C$, whose transition moment is along the chain direction and, consequently, this band is highly sensitive to changes in chain orientation. From the spectral data observed from Figure 7, we were able to confirm the following: for P(VDF−TrFE) thin films spin coated on a bare Au substrate, the comparatively lower B_1 ($\vec{\mu} \parallel \vec{c}$) band intensity indicates that the trans-planar zigzag chains tend to orient parallel to the substrate surface and the $\vec{a}$ and $\vec{b}$ axes are oriented away from the substrate surface as observed from higher absorbance intensity for A_1 and B_2. Au substrates modified with HDT and MHA too showed similar behavior. Among the two different SAMs used in this study, the absorbance ratio of the A_1 band to the B_2 band can actually be used to evaluate the extent to which the *b*-axis is perpendicular to the substrate and therefore contributes to the effective polarization. The two absorbance ratios of the A_1 band to the B_2 band, $A_{856cm^{-1}}/A_{895cm^{-1}}$ and $A_{1294\ cm^{-1}}/A_{1210cm^{-1}}$, of P(VDF−TrFE) films spin-coated on the HDT/Au substrate are lower than those observed for MHA/Au. This result is consistent with the structural analysis developed earlier: the lower absorbance corresponds to the (100) contact plane, i.e., the *b*-axis is oriented comparatively at a lower angle to the film surface, whereas the higher absorbance corresponds to the (110) contact plane face in which the *b*-axis is at some 60° to the film surface, i.e., at only 30° to the film normal.

2. Correlation of Film Structure with Substrate Polarity. Overall, the above structural analysis indicates that the P(VDF−TrFE) films deposited on SAM-modified and on bare Au have different contact planes, namely, (100) and (110). Although the

two planes have similar density of chains, their structure is different in view of the low symmetry of the P(VDF−TrFE) unit-cell. The underlying reason must of course reside in the nature of the interactions with the two surfaces. This issue can be tackled with the SAM-modified substrates in view of their intrinsic chemical versatility as well as the possibility to modify their structure by appropriate chemical reactions.

The structural analysis of the P(VDF−TrFE) films clearly establishes that the substrates can be divided in two classes that differ by their polarity. All the substrate modifications that rest on the use of the least polar, CH_3-terminated molecules (namely, OT, DDT, and HDT) result in a (100) contact face of the P(VDF−TrFE) film, i.e., the *b*-axis is parallel to the film surface. By contrast, the films deposited on bare Au have a (110) contact face parallel to the substrate.

The (110) contact face was also observed for films deposited on two very different, but both *polar* substrates. It was observed for the SAM made with a COOH-terminated molecule, namely, MHA (Figure 6d). In a different experiment, the hydrophobic HDT-modified-Au surface was turned into a hydrophilic one by a 30 s O_2 plasma treatment. The treatment significantly reduces the contact angle of water, to less than 30°. More importantly, the P(VDF−TrFE) deposited and annealed on this modified substrate has a (110) contact plane, i.e., is similar to the one formed on the bare and on the MHA-treated-Au surface (Figure 6e).

The above experimental results indicate that several rules govern the deposition of P(VDF−TrFE) copolymers on the various substrates. In essence: the chains lie parallel to the substrate, and the contact face is a densely packed crystallographic plane. These conditions leave only two different structural possibilities, namely, the (100) and the (110) contact planes. The orientation of the *c*-axis in the contact plane is random (all azimuthal angles are observed), evidenced by FESEM in Figure 1. This lack of selectivity may imply either the absence of any specific interactions such as epitaxy and preferred orientation by shear or that the SAMs are "polycrystalline" (made of crystalline domains with different orientations) at the resolution of the investigation technique used here (e.g., GIWAXS). Indeed, thin films and/or monolayers produced by, e.g., Langmuir−Blodgett techniques are usually polycrystalline, i.e., made of domains in which the *a*- and *b*-axes are randomly oriented in the plane of the films. More importantly, as a major novel outcome of the present investigation, the contact plane of the P(VDF−TrFE) film differs for apolar and polar substrate surfaces. It is (100) for the apolar, and (110) for the polar substrates, with bare Au belonging to this latter category.

These structural differences imply that the polarization vector (oriented parallel to the *b*-axis of the unit-cell) is differently oriented in the corresponding films. For the (100) contact face, the *b*-axis lies in the plane of the film, whereas it is at some 60° to the film surface for the (110) contact face. For optimal electric properties, it should be normal to the film surface. The (100) contact face is thus barely suitable, while the (110) contact face may be considered as acceptable. Indeed, the component normal to the film surface is reduced by only sin 60°, i.e., 0.87 of the maximum achievable value.

Ideally, a method should be devised that induces a (010) contact plane, i.e., that would orient the polarization vector normal to the film thickness. This, however, represents a considerable challenge. Indeed, the (010) plane is not a densely packed plane, since the chains are approximately 9 Å apart.[33] A weak or mildly specific interaction with the substrate is expected to induce a more dense contact face, namely, (100) or

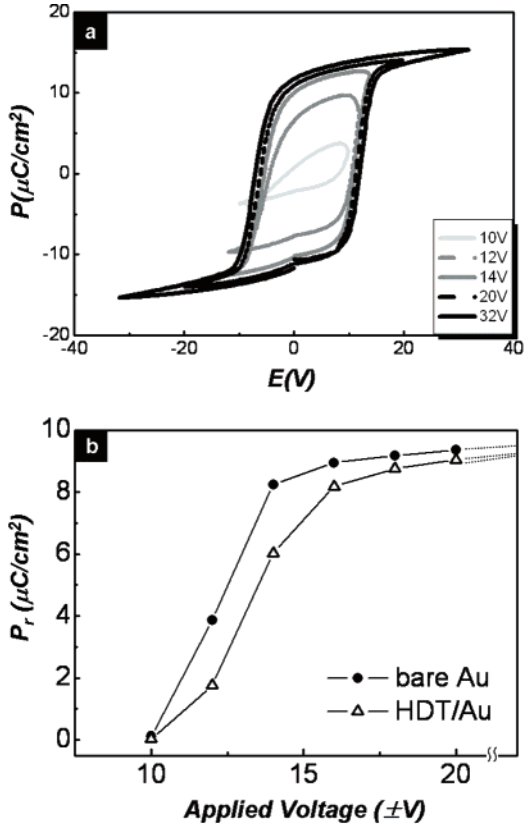

Figure 8. (a) Polarization *P* vs applied voltage *E* hysteresis loops of a 250 nm P(VDF−TrFE) polymer capacitor with a bare Au bottom electrode. (b) Plot of the remanent polarization P_r versus the applied voltage *E*. The slope between the P_r value and increasing applied voltage from 10 to 12 V is larger for the films deposited on bare Au than on the HDT-modified surface.

(110), as discussed above. To generate a less populated contact plane, say by epitaxial crystallization, the interactions must be more specific, with some form of structural matching with the (crystalline) substrate. Earlier investigations have shown that, provided a suitable dimensional lattice matching is achieved, epitaxial crystallization can induce unexpected contact planes. Most relevant in the present context is the epitaxial crystallization of polyethylene (PE) on various organic and inorganic substrates. Whereas the shortest interchain distances in PE are in the 4−5 Å range, contact planes with interchain distances larger than 9 Å were obtained.[34−36] For the present P(VDF−TrFE) polymers, and given the constraints set by the development of devices, resorting to exotic crystalline substrates (such as the salts of *p*-phenylbenzoic acid or phenylpenicillin used in the PE investigation) is however difficult to envisage.

3. Electric Properties and Modifications Induced by Electric Fields. The ferroelectric properties of P(VDF−TrFE) films depend to a large extent on the film characteristics, most prominently on the film thickness but also, as seen next, on the film structure. The ferroelectric properties have been evaluated after deposition on the top film surface of a layer of Al. First, we consider the properties of the films in general, before tackling the more subtle differences introduced by the two possible structures of the films considered above. In all cases, the films investigated have been spin coated and annealed at 135 °C for 2 h.

The film thickness has a significant influence, as shown by the very different remanent polarization (P_r) and coercive voltage (V_c) in a saturated hysteresis curve. A typical ferroelectric hysteresis loop for a film deposited on a bare Au surface is

shown in Figure 8a. When an increasing voltage is applied on the capacitor, the remanent polarization and coercive voltage increase and saturation is reached when the voltage is above ±20 V. Under these conditions (i.e., >±20 V), for a 250 nm P(VDF−TrFE) film, P_r and V_c are 8.2 μC/cm^2 and 12 V, respectively, corresponding to a coercive electric field (E_c) of approximately 50 MV/m, which is consistent with values reported earlier in the literature (Table 2). Films that are 110 nm thick have a lower V_c (approximately 9 V), corresponding to an E_c of approximately 80 MV/m. The increase in E_c with decreasing film thickness is usually attributed to hindered chain mobility. For even thinner films (70 nm) a very low switching voltage of 4.95 V is recorded. This corresponds however to a practical limit, since further reduction of the film thickness results in a significantly reduced polarization, to be associated with the reduced crystallinity. Actually, ultrathin P(VDF−TrFE) films (only 30 nm thick) frequently show electric shortage, mainly due to the insufficient film coverage, as observed in Figure 1.

The above experiments all rest on the application of electric fields above 20 V, that is, and deal with saturated hysteresis curves. This in turn indicates that an electric bias of about 80 MV/m applied to the film, is sufficient to "switch" polymer chains, that is, to induce rotation of the chains on their axis. Such high electric fields would "wipe out" the structural differences that have been uncovered in the films deposited on Au and on SAM-modified Au, since these rest indeed *only* on the orientation of the chains on their axis. In order to investigate the impact of the structural differences on the ferroelectric properties, significantly lower voltages should be applied to the films.

The experimental procedure used to investigate the films deposited on Au and SAM-modified ones depends therefore on the same procedure as before but focuses on the variation of the P_r after application of voltages in the 10−15 V range. Figure 8b compares the remanent polarizations for the bare and SAM-modified films. The evolution of P_r versus applied voltage looks at first sight very similar: steep increase for the 10−15 V range and saturation at about 20 V. On further inspection, however, the bare and SAM-modified films show actually a different response to the applied voltage. Indeed, in the steepest part of the curve, in the critical 10−15 V range, the remanent polarization of the SAM-modified is, for any given applied voltage, approximately 2 μC/cm^2 lower. Of course, and as already discussed, all P(VDF−TrFE) thin films, regardless of the substrate type, have similar remanent polarization when the applied voltage reaches 20 V.

The observed differences in the remanent polarizations values can be related with the structure of the thin films, at least qualitatively, since the analysis cannot take into account the various structural disorders discussed earlier (lamellar twisting, reorientation of the *a*-axis during growth through the film thickness). In brief, the ferroelectric response to the electric bias in the P(VDF−TrFE) films depends on the amount of the polar *b*-axis that is normal to the film (or, in the case of tilted *b*-axis, on its projection onto the film normal). The films deposited on bare Au and SAMs-modified substrates are very different in this respect. In films deposited on bare Au, and sticking to the cell orientation near the contact plane, the polar *b*-axis is oriented at only 30° to the surface normal, which implies that the contribution is cos 30° of the maximum achievable polarization. On the contrary, the films deposited on SAM-modified Au have the worse cell orientation, with the polar *b*-axis in the plane of the film, i.e., at right angles to their optimal orientation. (This of course does not apply for the MHA substrate, with its COOH end group).

Conclusion

We have investigated the molecular and microstructure of semicrystalline P(VDF−TrFE) thin films deposited on a bare Au substrate and a modified one with a SAM interlayer as a function of both film thickness and surface property of the Au or SAM interlayer. In all films, the *c*-axis is oriented in the contact plane, that is, parallel to the substrate. No azimuthal orientation preference can be detected, which may result either from the absence of specific interactions or from the fact that, especially with SAMs, the domain size of the interlayer is below the resolution of the investigation technique. The films deposited on bare Au and on polar SAMs are characterized by a (110) contact plane, whereas those deposited on CH_3-terminated SAMs have a (100) contact plane, which implies that the P(VDF−TrFE) *b*-axis of the unit-cell is either tilted at some 30° to the film surface normal or lies in the plane of the film. Furthermore, specificities of the GIWAXS patterns suggest that the polymer lamellae twist in space, as is frequently observed in polymer crystal growth. The different unit-cell orientations of the films are manifested by different remanent polarizations when the films are submitted to relatively low voltages of 10∼15 V, i.e., that remain below the coercive voltage in the thin films investigated. When the films are submitted to >20 V, molecular reorientation in the films wipes out these structural differences to a significant extent. Interestingly however, the films produced on both polar and apolar substrates have densely populated contact planes. This implies that the sole reorientation of the chains by rotation on their axis under a coercive electric field generates at best a structure in which the polar *b*-axis is oriented at 30° to the electric field. Further alignment of the *b*-axis to bring it parallel to the electric field would require energetically more demanding shifts of whole molecules in the film, in essence it would require a 30° rotation of the whole crystal lattice in order to bring the densely populated *bc* plane of the unit-cell normal rather than parallel to the film surface and reciprocally for the less densely populated *ac* plane.

To conclude, the present investigation has indicated that the ferroelectric properties of the P(VDF−TrFE) films depend, in addition to the film thickness, on their detailed structural/morphological organization, which itself depends on the hydrophobic/hydrophilic character of the substrates on which they are deposited.

Acknowledgment. This project was supported by The National Research Program for the 0.1 Terabit Non-Volatile Memory Development and "SYSTEM2010" project sponsored by Korea Commerce, Industry and Energy and Samsung Electronics, Co., Ltd. The X-ray experiments at PAL (4C2 beamline), Korea, were supported by MOST and POSCO, Korea. This work was supported by the Second Stage of Brain Korea 21 Project in 2006, Seoul Science Fellowship, the Korea Research Foundation Grant funded by the Korean Government (MOEHRD) (KRF-2006-612-D00027) and the Korea Science and Engineering Foundation (KOSEF) grant funded by the Korea government (MOST) (No. R11-2007-050-03001-0).

References and Notes

(1) Ducharme, S.; Reece, T. J.; Othon, C. M.; Rannow, R. K. *IEEE Trans. Device Mater. Reliab.* **2000**, *5*, 720.
(2) Naber, R. C. G.; Tanase, C.; Blom, P. W. M.; Gelinck, G. H.; Marsman, A. W.; Touwslager, F. J.; Setayesh, S.; De Leeuw, D. M. *Nat. Mater.* **2005**, *4*, 243.

(3) Gelinck, G. H.; Marsman, A. W.; Touwslager, F. J.; Setayesh, S.; De Leeuw, D. M.; Naber, R. C. G.; Blom, P. W. M. *Appl. Phys. Lett.* **2005**, *87*, 092903.
(4) Dargaville, T. R.; Celina, M.; Chaplya, P. M. *J. Polym. Sci., Polym. Phys. Ed.* **2005**, *43*, 1310.
(5) Zhu, G.; Zeng, Z.; Zhang, L.; Yan, X. *Appl. Phys. Lett.* **2006**, *89*, 102905.
(6) Fujisaki, S.; Ishiwara, H.; Fujisaki, Y. *Appl. Phys. Lett.* **2007**, *90*, 162902.
(7) Xu, H.; Zhong, J.; Liu, X.; Chen, J.; Shen, D. *Appl. Phys. Lett.* **2007**, *90*, 092903.
(8) Park, Y. J.; Kang, S. J.; Kim, K. J.; Lee, H. S.; Lee, M. S.; Chung, U.-I.; Park, I. J.; Park, C. *Appl. Phys. Lett.* **2006**, *88*, 242908.
(9) Urayama, K.; Tsuji, M.; Neber, D. *Macromolecules* **2000**, *33*, 8269.
(10) Xia, F.; Xu, H. H.; Razavi, B.; Cheng, Z.-Y.; Zhang, Q. M. *J. Appl. Phys.* **2002**, *92*, 3111.
(11) Xia, F.; Zhang, Q. M. *Appl. Phys*. Lett. **2004**, *85*, 1719.
(12) Park, Y. J.; Kang, S. J.; Woo, E.; Shin, K.; Kim, K. J.; Park, C. *Appl. Phys. Lett.* **2007**, *90*, 222903.
(13) Yan, C.; Zharnikov, M.; Golzhauer, A.; Grunze, M. *Langmuir* **2000**, *16*, 6208.
(14) Chong, L. W.; Lee, Y. L.; Wen, T. C.; Guo, T. F. *Appl. Phys. Lett.* **2006**, *89*, 233513.
(15) Khodabaksh, S.; Sanderson, B. M.; Nelson, J.; Jones, T. S. *Adv. Funct. Mater.* **2005**, *16*, 95.
(16) Robel, I.; Subramanian, V.; Kuno, M.; Kamat, P. V. *J. Am. Chem. Soc.* **2006**, *128*, 2385.
(17) Kim, D. H.; Park, Y. D.; Jang, Y.; Yang, H.; Kim, Y. H.; Han, J. I.; Moon, D. G.; Park, S.; Chang, T.; Chang, C.; Joo, M.; Ryu, C. Y.; Cho, K. *Adv. Funct. Mater.* **2005**, *15*, 77.
(18) de Boer, B.; Hadipour, A.; Mandoc, M. M.; van Woudenbergh, T.; Blom, P. W. M. *Adv. Mater*. **2005**, *17*, 621.
(19) Hwang, J.; Huh, J.; Jung, B.; Hong, J.-M.; Park, M.; Park, C. *Polymer* **2005**, *46*, 9133.
(20) Li, J.; Luo, Y.; Bai, M.; Ducharme, S. *Appl. Phys. Lett.* **2005**, *87*, 213116.
(21) Bai, M.; Ducharme, S. *Appl. Phys. Lett.* **2004**, *85*, 3528.
(22) Wang, J.; Li, H.; Liu, J.; Daun, Y.; Jiang, S.; Yan, S. *J. Am. Chem. Soc*. **2003**, *125*, 1496.
(23) Lovinger, A. *Polymer* **1981**, *22*, 412.
(24) Bellet-Amalric, E.; Legrand, J. F. *Eur. Phys. J. B* **1998**, *3*, 225.
(25) *Cerius*^{2}; Diffraction Faulted Module of the Cerius^2 package; Accelrys: San Diego, CA, .
(26) Lotz, B.; Cheng, S. Z. D. *Polymer* **2005**, *46*, 577.
(27) Toda, A.; Arita, T.; Hikosaka, M. *Polymer* **2001**, *42*, 2223.
(28) Gregorio, R., Jr.; Capitao, R. C. *J. Mater. Sci.* **2000**, *35*, 299.
(29) Vaughan, A. S. *J. Mater. Sci.* **1993**, *28*, 1805.
(30) Lotz, B.; Thierry, A.; Schneider, S. *C. R. Acad. Sci., Ser. IIc* **1998**, 609.
(31) Hasegawa, R.; Takahashi, Y.; Chantani, Y.; Tadokoro, H. *Polym. J.* **1972**, *3*, 600.
(32) Bain, C. D.; Troughton, E. B.; Tao, Y.-T.; Evall, J.; Whitesides, G. M.; Nuzzo, R. G. *J. Am. Chem. Soc.* **1989**, *111*, 321.
(33) Prabu, A. A.; Lee, J. S.; Kim, K. J.; Lee, H. S. *Vib. Spectrosc.* **2006**, *41*, 1.
(34) Wittman, J. C.; Lotz, B. *Prog. Polym. Sci.* **1990**, *15*, 909.
(35) Wittman, J. C.; Lotz, B. *J. Polym. Sci., Polym. Phys. Ed.* **1981**, *19*, 1837.
(36) Wittman, J. C.; Hodge, A. M.; Lotz, B. *J. Polym. Sci., Polym. Phys. Ed.* **1983**, *21*, 2495.

MA0718705